Article

Evolution of Physical and Mechanical Properties of Granite after Thermal Treatment under Cyclic Uniaxial Compression

Bo Hu [1], Xiangqi Hu [1], Chenggeng Lin [1], Guangzhen Du [1], Tianxing Ma [2] and Kaihui Li [1,*]

1   School of Resources and Safety Engineering, Central South University, Changsha 410083, China; hubocsu@163.com (B.H.)
2   Ocean College, Zhejiang University, Zhoushan 316021, China
*   Correspondence: geokhli@csu.edu.cn or kaihuili_csu@163.com

Abstract: The combined effects of thermal and cyclic loading result in complex mechanical behavior in engineering rock masses. The study of the physical and mechanical properties of these rock masses is of great importance for improving the stability and sustainability of structures built on thermally treated rock masses. In order to understand the failure mechanism, uniaxial compression tests and cyclic loading and unloading tests were conducted on granite specimens that had undergone thermal treatment at various temperatures. The test results indicate that the density and P-wave velocity of the specimens decrease while the degree of damage increases after thermal treatment. The compressive strength and elastic modulus of the specimens generally decrease as a result of thermal treatment, although thermal hardening does occur within the temperature range of 200–400 °C. The dilatancy characteristics of the specimens change with the treatment temperature, and they are more prone to shear dilation under external loading. Furthermore, the failure mode of the specimens transitions from brittle to ductile failure as the treatment temperature increases. The combination of thermal treatment and cyclic loading causes the rock fragments to become looser and finer following specimen failure.

Keywords: coupled effect; cyclic loading; rock mechanics; thermal treatment

1. Introduction

Temperature is a crucial factor that influences the mechanical properties of rocks [1]. The impact of high temperature on rock mass cannot be disregarded in various deep rock underground engineering applications such as deep mining, high-temperature nuclear waste storage, shale gas exploration, enhanced geothermal system (EGS) development, and deep oil drilling [2–7]. Furthermore, the deep surrounding rock often exhibits complex mechanical behavior and may even lead to geological disasters such as rock bursts, tunnel water inrushes, shaft instabilities, and earthquakes due to disturbances caused by engineering loads like blasting vibration and mechanical excavation [8–16]. Therefore, ensuring the safety and stability of deep underground resource development and maximizing the utilization of deep underground space have become significant topics in the field of rock mechanics [17].

In recent years, numerous laboratory tests have been conducted to investigate thermal effect on the mechanical properties of rocks. Some of these studies focused on the physical and mechanical properties of rocks under high-temperature conditions in real-time, while others focused on the properties after cooling following high-temperature treatment. These studies have yielded a series of results. For instance, Kumari et al. [18] conducted triaxial compression tests on Australian Strathbogie granite at various confining pressures and real-time temperatures. They observed the damage characteristics of rock samples using an acoustic emission (AE) system. At temperatures below 200 °C, the expansion of mineral crystals inhibited the formation of microcracks. However, at temperatures above 400 °C,

microcracks formed along grain boundaries, resulting in thermal damage. This observation was further supported by the results of SEM analysis. In another study, Xu et al. [19] investigated the influence of two factors, namely real-time high temperature and loading rate, on the fracture mode of granite. They found that as the temperature increased, the deformation and failure mode of granite transitioned from tensile shear fracture to conical fracture, accompanied by a shift towards cataclastic flow. In contrast, the change in loading rate at the same temperature did not have a significant influence on the fracture mode. Gautam et al. [20] conducted a study on Indian Jalore granite after subjecting it to thermal treatment at various temperatures. They combined the results of uniaxial compression tests with a large number of scanning electron microscope (SEM) images. The researchers observed that the temperature range of 300–600 °C represented the brittle–ductile transition zone of granite. They also found that a phase transition occurred when the temperature reached a specific critical value, typically above 300 °C. Additionally, even a slight increase in temperature resulted in the formation of numerous thermal cracks, which weakened the grain structure and transformed the granite from brittle to ductile. Wu et al. [21] investigated the impact of cooling rate on the mechanical properties of granite after thermal treatment at different temperatures using the Brazilian splitting test. The findings indicate that rock samples that experienced faster cooling rates were more susceptible to thermal shock. Additionally, the cooling rate had minimal impact on the tensile strength of the rock samples below 400 °C. However, when the temperature exceeded 600 °C, the tensile strength of the rock samples decreased significantly with increasing cooling rate. Yin et al. [22] conducted real-time static uniaxial compression tests to compare and analyze the mechanical properties of granite under high-temperature conditions, as well as after heating and cooling. The results revealed that the peak stress and elastic modulus of granite decreased, while the critical temperature of the brittle–ductile transition increased after thermal treatment compared with real-time thermal treatment.

In addition, cyclic loading tests are considered an effective method for studying the fatigue and dynamic properties of rocks [23]. These tests can be divided into two categories: fatigue loading tests and graded cyclic loading tests. The mechanical properties of rock materials under cyclic loading differ from those under static loading due to variations in mineral content, texture, and microstructure [24]. Therefore, it is important to conduct experimental research on the cyclic loading of rocks while considering the effect of temperature, as this has both theoretical and practical significance. However, most experimental studies on the effects of cyclic loading on the mechanical properties of rocks are conducted at normal temperatures, with only a few considering real-time temperature or thermal treatment. For example, Jia et al. [25] conducted fatigue loading tests on granite, marble, and greenstone that had been cooled using water at high temperatures. It has been observed that as the number of cycle times increases, the plastic deformation of the three types of rock samples decreases, the elastic modulus increases, and the failure strength exceeds the uniaxial compressive strength. Additionally, as the temperature increases, the elastic moduli of the three types of rock samples decrease, while the peak strain increases. Xia et al. [26] conducted a cyclic uniaxial stress–temperature test on basalt and found that cyclic stress and cyclic temperature had a superposition effect. When the upper limit of cyclic stress reached 80% of the uniaxial compressive strength, the basalt gradually experienced damage until it was ultimately destroyed with an increasing number of stress–temperature cycles. However, when the upper limit of cyclic stress was 65% of the compressive strength and the upper limit of temperature was 60 °C, the basalt exhibited a "hardening" phenomenon with an increasing number of cycles, and no damage occurred. Zhao et al. [27] conducted a comprehensive study of the effects of temperature and unloading stress levels on the mechanical properties and energy characteristics of granite using a stepped-increase cyclic load test under real-time temperature conditions. The experimental results demonstrated that the strength of the rock sample was enhanced by the cyclic load when the temperature was below 600 °C. Moreover, as the temperature increased, the energy evolution of the granite transitioned from nonlinear to linear. Additionally, the elastic modulus and

maximum strain exhibited an increase with the escalation of the unloading stress level. Han and Li [28] conducted uniaxial tensile and cyclic tensile tests on marble samples that were subjected to varying temperatures. The findings indicated that the tensile strength of the rock samples decreased as the treatment temperature increased, and this decrease was linearly correlated with the longitudinal wave velocity. Furthermore, the cyclic tensile stress did not have a significant impact on the tensile strength.

All the aforementioned studies have examined the effects of temperature and cyclic loading on the mechanical properties of rocks from various perspectives. However, due to the limited number of such studies, the results are insufficient for a comprehensive understanding of the complex mechanical behavior of surrounding rock in deep-rock geothermal engineering; therefore, further basic research in this area is still necessary. To date, there have been few reports on the mechanical properties of rocks following thermal treatment, cooling, and subsequent testing under uniaxial graded cyclic loading. Additionally, most previous experimental studies have only explored temperatures up to 600 °C, leaving a gap in research on the mechanical properties of rocks subjected to high-temperature treatment ranging from 600 °C to 1000 °C. In light of this background, in the present study, we conducted graded cyclic loading and unloading tests on granite samples that were treated at different temperatures (ranging from 25 °C to 1000 °C). The study aimed to analyze the relationships between stress-strain, peak strength, crack damage threshold, elastic properties, deformation, and failure characteristics of granite in relation to thermal temperature. It will provide a reference for understanding the fracture mechanism of surrounding rocks in similar engineering projects, ensuring the stability and reliability of high-temperature rock underground engineering and promoting the development and utilization of geothermal energy.

2. Test Materials and Test Methods

2.1. Sample Preparation

The granite samples utilized in the experiment were obtained from Baishi Town, Jining City, Shandong Province, China. In order to minimize variations, all the samples were sourced from the same parent rock that possessed a consistent texture and lacked any visible joints or cracks. The granite block was then processed into cylindrical shapes with dimensions of φ50 mm $\times$ L100 mm. The flatness of the end face of each specimen was carefully controlled to be within $\pm$0.02 mm, in accordance with the recommendations provided by the ISRM [29]. This is illustrated in Figure 1. The average natural density and P-wave velocity of all the samples were determined to be 2.585 g/cm^3 and 4266 m/s, respectively.

Figure 1. Prepared granite samples.

In this study, the sample underwent thermal treatment in an SX2-10-12MP box-type resistance furnace. The resistance furnace has a maximum working temperature of 1200 °C and a rated power of 10 kW. To establish temperature gradients, six predetermined temperature groups were set: 25 °C (room temperature), 200 °C, 400 °C, 600 °C, 800 °C, and 1000 °C. Each group consisted of six samples. Each sample was placed in the furnace and heated to the predetermined temperature at a rate of 5 °C/min. Once the predetermined temperature was reached, the sample was maintained at a constant temperature for 4 hours to minimize thermal damage caused by uneven heating [30]. The sample was removed from the furnace after natural cooling to room temperature to prevent thermal shock, and its basic physical parameters were promptly determined. Additionally, the apparent morphological damage of the sample was recorded and analyzed [31]. Mechanical tests were conducted on the specimens after thermal treatment.

2.2. Test Equipment and Methods

The YZW100 multifunctional rock direct shear instrument at Central South University was utilized as the loading equipment, with a maximum working pressure of 500 kN, as shown in Figure 2. The mechanical test was divided into two groups: a conventional uniaxial compression test and a constant lower limit cyclic loading and unloading test. Each group of tests included three samples. The loading method for the tests was as follows.
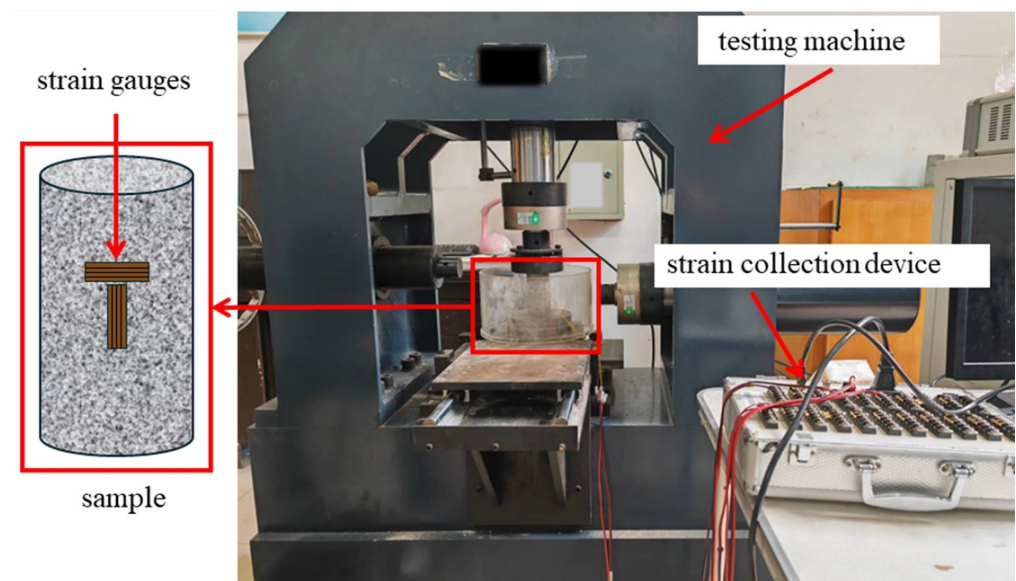

Figure 2. Test equipment and strain gauge layout.

1. Conventional uniaxial compression test

The compression load was applied in displacement control mode, at a loading rate of 0.004 mm/s, until the sample reached its point of failure. This experiment aimed to investigate the fundamental physical and mechanical properties of thermally treated granite specimens under conventional uniaxial compression.

2. Constant lower limit cyclic loading and unloading test

To facilitate the execution of multiple cyclic loading and unloading tests on samples subjected to different thermal treatments, a test scheme was devised. This scheme involved applying a constant lower limit under gradient loading, specifically axial displacement. The loading rate was set at 0.004 mm/s and a loading gradient of 0.1 mm was employed for each cycle. Once the specimen reached the designated axial displacement, the axial stress was unloaded using displacement control mode at a rate of 0.004 mm/s. This cycle was repeated until the sample incurred damage. It is important to note that unloading

was halted when the axial stress reached 1 MPa to maintain contact between the sample's end face and the loading platen throughout the test. The stress path for the constant lower limit cyclic loading and unloading test is depicted in Figure 3. This experiment aimed to investigate the mechanical properties and thermal damage evolution of granite samples following thermal treatment under cyclic loading.
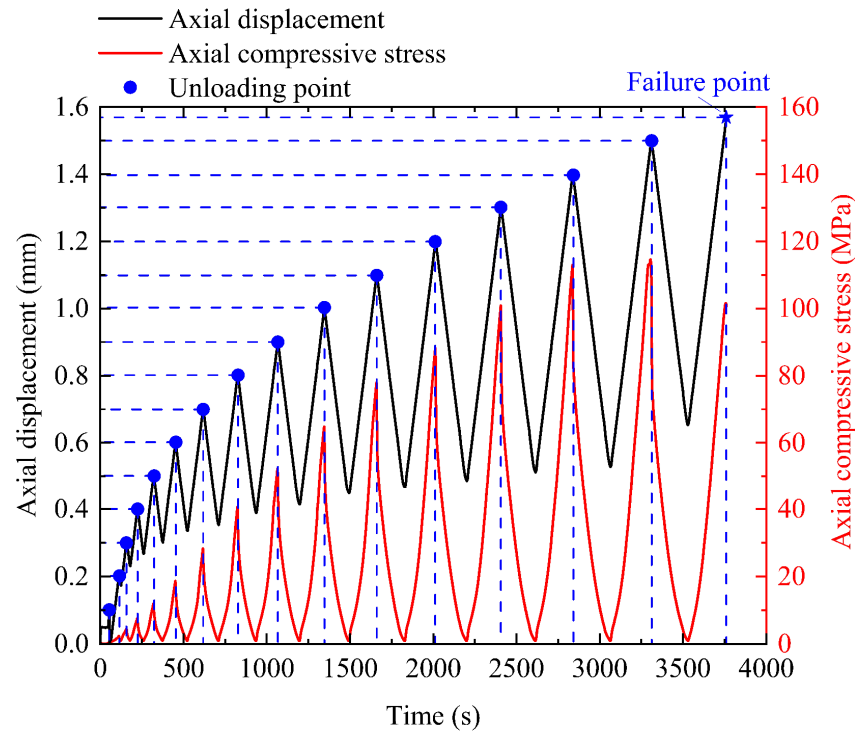

Figure 3. The cyclic loading path for samples.

3. Thermally Induced Changes in Physical Properties

3.1. Mass, Volume, and Density

Mass, volume, and density are significant indicators that demonstrate alterations in the composition of rock materials following thermal treatment. In order to examine the impact of thermal treatment on granite mass, volume, and density, the mass loss rate K_m, the volume growth rate K_v, and the density loss rate K_ρ were defined as:

$$K_m = \frac{m_0 - m_T}{m_0} \times 100\% \tag{1}$$

$$K_v = \frac{V_0 - V_T}{V_0} \times 100\% \tag{2}$$

$$K_\rho = \frac{\rho_0 - \rho_T}{\rho_0} \times 100\% \tag{3}$$

where m_0 and m_T are the masses of the sample before and after thermal treatment, respectively; V_0 and V_T are the volumes of the sample before and after thermal treatment, respectively; and ρ_0 and ρ_T are the densities of the sample before and after thermal treatment, respectively. It should be noted that the above indicators were measured at normal temperature and pressure.

Figure 4 illustrates the impact of treatment temperature on both the mass loss and mass loss rate. As the treatment temperature increases, both mass loss and mass loss rate exhibit an upward trend; the mass loss rate can be categorized into three stages. In the first stage, the mass loss rate increases by 0.10% in the temperature range of 25–200 °C. In the second

stage, the rate of mass loss growth slows down and experiences a 0.02% increase as the temperature ranges from 200 °C to 400 °C. In the third stage, within the temperature range of 400–1000 °C, the growth rate of mass loss increases and stabilizes, with a change of 0.09%. The variation in the mass loss rate during the first phase is dependent on the free water content present in the sample. As the heating process progresses, the free water gradually converts into steam and escapes through the open pores, resulting in mass loss. This outcome aligns with the findings of Zuo et al. [32]. With increasing treatment temperature, a small amount of bound water within the rock is released, leading to a decrease in mass in the second stage. This finding is consistent with the results obtained by Wu et al. [33]. The reasons for the change in the rate of mass loss during the third stage are more complex. First, the water present in the mineral structure precipitates and vaporizes, resulting in a decrease in mass [34]. Second, the thermal expansion of mineral particles induces thermal stress, which weakens the adhesion between particles. As a result, some particles detach from the surface of the specimen, leading to a decrease in mass. Additionally, the thermal decomposition of granite within this temperature range also contributes to the decrease in mass [35].
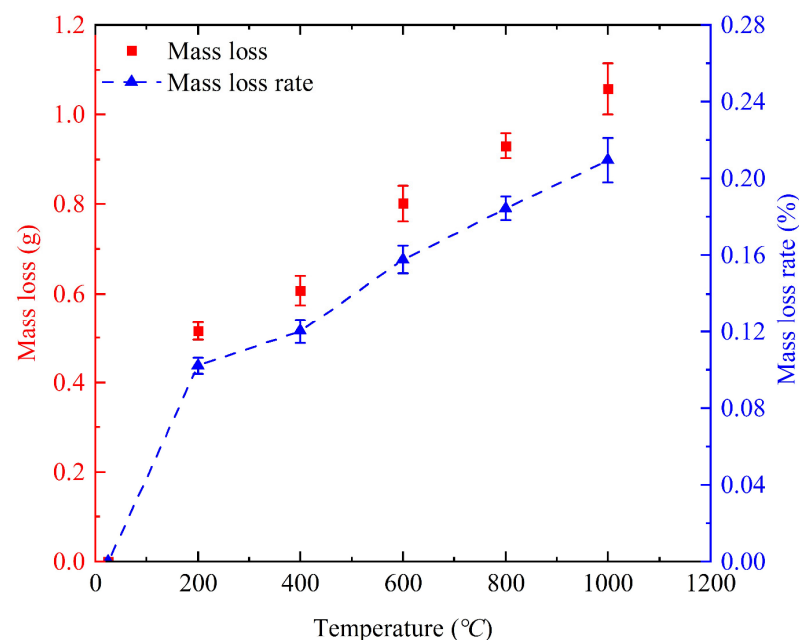

Figure 4. Variation in mass loss and mass loss rate with treatment temperature.

The trends of volume expansion and volume expansion rate with temperature are illustrated in Figure 5. Below 400 °C, the volume expansion rate remains relatively stable. However, beyond 400 °C, the volume expansion rate experiences a rapid increase. This can be attributed to the fact that within the temperature range of 25–400 °C, the initial porosity of the rock causes the expansion extrusion of mineral particles to primarily compact the primary pore space without generating new microcracks. Consequently, the volume expansion rate undergoes minimal change during this stage. The transition from the α phase to the β phase occurs at approximately 573 °C, leading to an anisotropic thermal expansion that significantly accelerates the initiation and expansion of thermally induced microcracks. As a result, the volume expansion rate experiences a substantial increase within the range of 400–1000 °C [36].
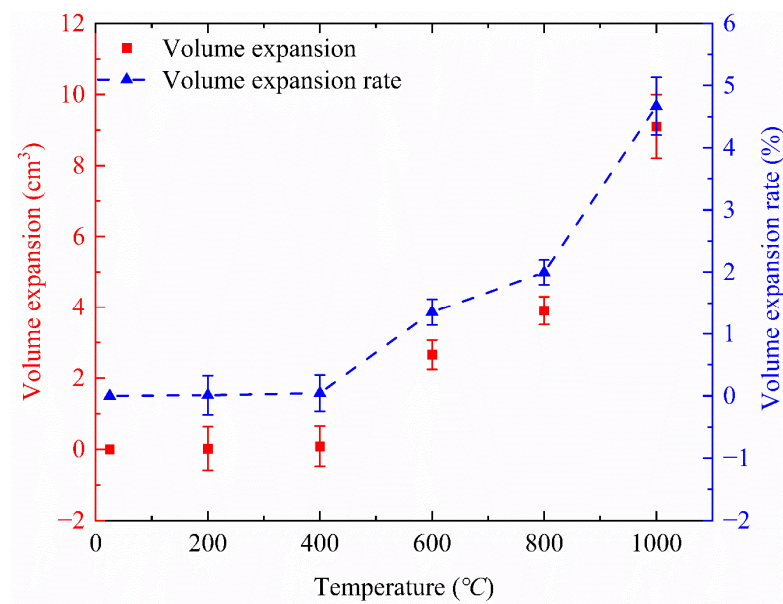
Figure 5. Variation in volume expansion and volume expansion rate with treatment temperature.

Since the rate of mass loss in granite is relatively small compared with the rate of volume increase, the rate of density loss in the sample changes in a similar manner to the rate of volume increase, as depicted in Figure 6. It is evident that the rate of density loss remains constant within the temperature range of 25–400 °C. However, when the temperature exceeds 400 °C, the rate of density loss starts to increase rapidly, indicating a gradual loosening of the overall structure of the sample. Furthermore, the relationship between the rate of density loss and temperature can be accurately described by an exponential function, which aligns with the findings of Zhao et al. [37].
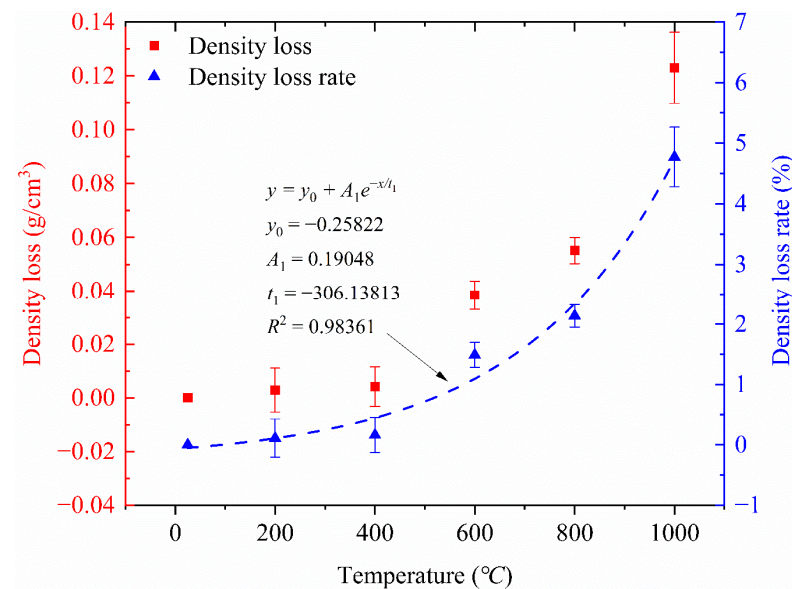

Figure 6. Variation in density loss and density loss rate with treatment temperature.

3.2. P-Wave Velocity

Wave velocity is highly responsive to microcracks in rock samples and is commonly employed to assess the extent of thermal damage resulting from thermal treatment [38]. In this investigation, a HS-YS4A type rock acoustic parameter tester was utilized to measure the P-wave velocity of all samples both before and after thermal treatment. The alterations

in the P-wave velocity, P-wave velocity attenuation rate, and damage factors subsequent to thermal treatment at various temperatures are presented in Figure 7.
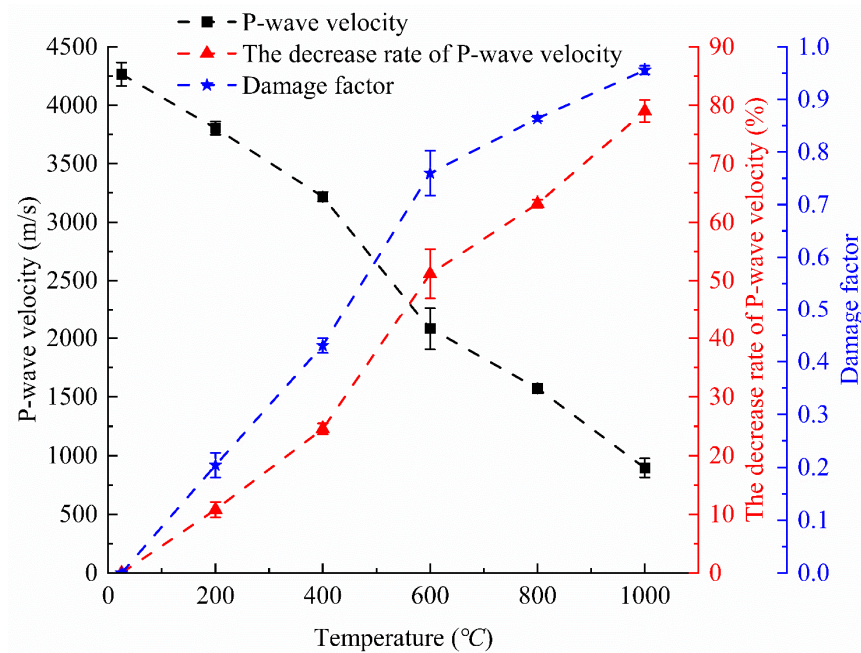

Figure 7. Variation in P-wave velocity and P-wave velocity decrease rate with temperature.

The rate of change in wave velocity is determined using the following formula:

$$K_p = \frac{v_{p0} - v_{pT}}{v_{p0}} \times 100\% \tag{4}$$

where v_{p0} and v_{pT} are the P-wave velocities of a specimen before and after thermal treatment, respectively.

The damage factor associated with P-wave velocity is calculated based on reference [39]:

$$D_{vp} = 1 - \left(\frac{v_{pT}}{v_{p0}} \right)^2 \tag{5}$$

The thermal treatment significantly affects the P-wave velocity of the sample. As the treatment temperature increases, the P-wave velocity gradually decreases. However, there is a sharp decrease in velocity between 400 °C and 600 °C. Additionally, the damage factor increases significantly primarily due to the formation of microcracks caused by the thermal expansion of mineral particles that hinder the propagation of P-waves in the sample [40]. When the treatment temperature exceeds 600 °C, the decay rate of P-wave velocity slows down. This indicates that the thermal treatment induces less new damage to rocks. These findings are consistent with the test results of Zhao et al. [37] and Zhi et al. [41].

4. Thermally Induced Changes in Mechanical Properties

4.1. Stress-Strain Curves

It is important to note that the post-peak section of the stress-strain curve could not be captured in this study. This was because the granite samples experienced brittle failure during both the uniaxial compression test and the cyclic loading test. Additionally, the effect of confining pressure was not taken into account during loading.

Typical stress-strain curves of specimens subjected to thermal treatment at various temperatures under uniaxial compression are presented in Figure 8, where σ_1 is the axial stress, ε_1 is the axial strain, and ε_3 is the lateral strain. The uniaxial compressive stress-strain curve of the sample can be divided into three stages: initial compaction, elasticity, and

yield. However, due to the dense nature of the granite used in this study, the yield stage is not evident. As the treatment temperature increases, the nonlinear compaction stage of the curve is prolonged and the proportion of the elastic deformation stage gradually decreases. This is because the thermal damage leads to the formation of defects such as microcracks, pores, and dislocations, which in turn increase the development of initial cracks in the sample [42]. In addition, thermal treatment significantly affects the strength and deformation characteristics of the sample. Specifically, when the treatment temperature ranges from 25 °C to 400 °C, the compressive strength of the sample decreases. On the other hand, when the treatment temperature ranges from 400 °C to 1000 °C, both the compressive strength and Young's modulus of the specimen noticeably deteriorate, while the ductility of the specimen improves. This can be attributed to the phase transition of granite mineral particles around 600 °C and the resulting thermally induced microstructure.
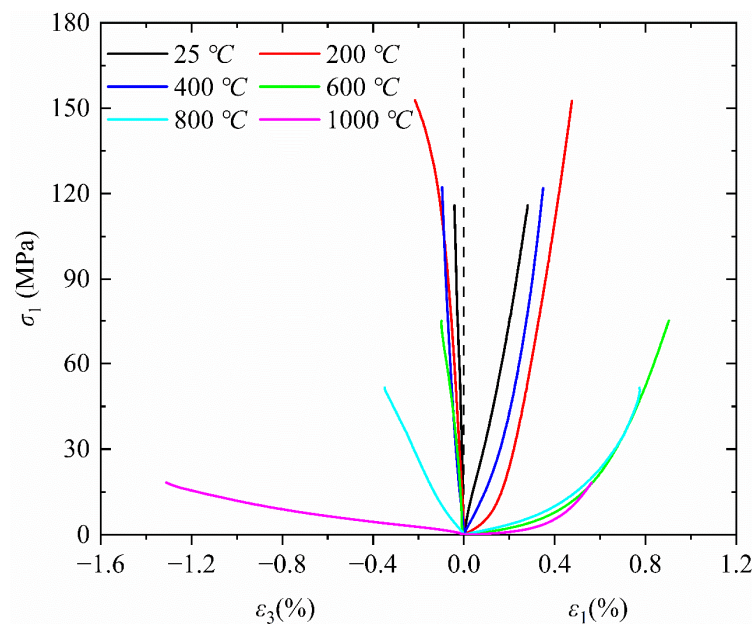

Figure 8. Typical stress-strain curves obtained from uniaxial compression tests of samples treated at different temperatures.

Figure 9 illustrates the typical stress-strain curves of specimens subjected to thermal treatment at various temperatures under cyclic loading. The stress-strain curve in the cyclic loading test exhibits a noticeable hysteresis effect. This means that the unloading curve does not align with the original loading curve, and a closed hysteresis loop is formed with the subsequent cyclic loading curve. This phenomenon is considered the manifestation of energy dissipation [43]. The dissipated energy is utilized for crack initiation, propagation, and coalescence, and is directly proportional to the area enclosed by the hysteresis loop [44,45]. It is observed that as the number of cycles increases, the hysteresis loops exhibit a pattern of sparse–dense–sparse distribution. Additionally, the area of the hysteresis loop significantly increases, indicating an increase in the degree of damage to the sample. It is worth noting that as the treatment temperature increases, the loading and unloading curves become sparser. This suggests that the sample, after undergoing thermal treatment, experiences greater plastic deformation and higher energy dissipation per cycle. Consequently, microcracks become interconnected and coalesce to form macroscopic cracks. As a result, the bearing capacity of the sample decreases while the deformation capacity increases. If the peak stress is not reached in subsequent cycles, significant plastic deformation can continue until failure occurs.
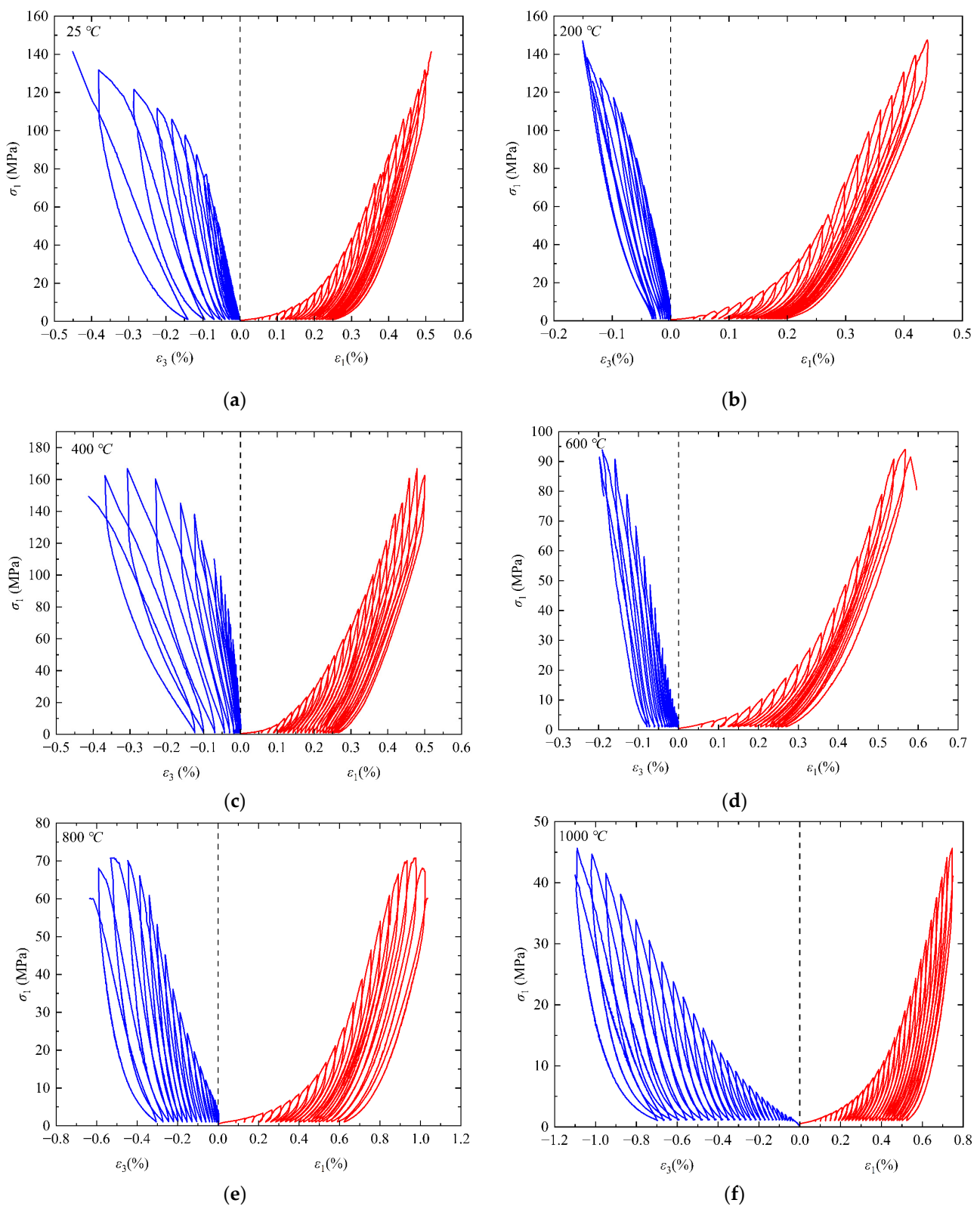
Figure 9. Typical stress-strain curves obtained from uniaxial cyclic loading tests of samples heated at different temperatures. (**a**) 25 °C; (**b**) 200 °C; (**c**) 400 °C; (**d**) 600 °C; (**e**) 800 °C, and (**f**) 1000 °C.

4.2. Compressive Strength

Figure 10 illustrates the variation in compressive strength of the sample as a function of treatment temperature. In the uniaxial compression test, the compressive strength of the

sample decreases from 140.23 MPa at 25 °C to 15.76 MPa at 1000 °C, representing a decrease of 88.8%. This indicates that treatment at high temperatures significantly deteriorates the strength of granite. However, it is worth noting that the compressive strength does not consistently decrease with increasing treatment temperature. At a treatment temperature of 200 °C, the compressive strength increases to 155.64 MPa, reflecting an increase of 11.0%. This phenomenon of thermal hardening has also been observed in experiments conducted by Rao et al. [46] and Sirdesai et al. [47]. The compaction of rock structures is widely recognized as the primary mechanism for thermal hardening. When subjected to thermal treatment at lower temperatures, rock grains experience moderate expansion, leading to the closure of initial microcracks and the formation of a denser structure [48,49]. It is important to note that thermal damage only occurs when the treatment temperature surpasses the critical threshold, which is contingent upon the initial porosity of the rock sample [50].
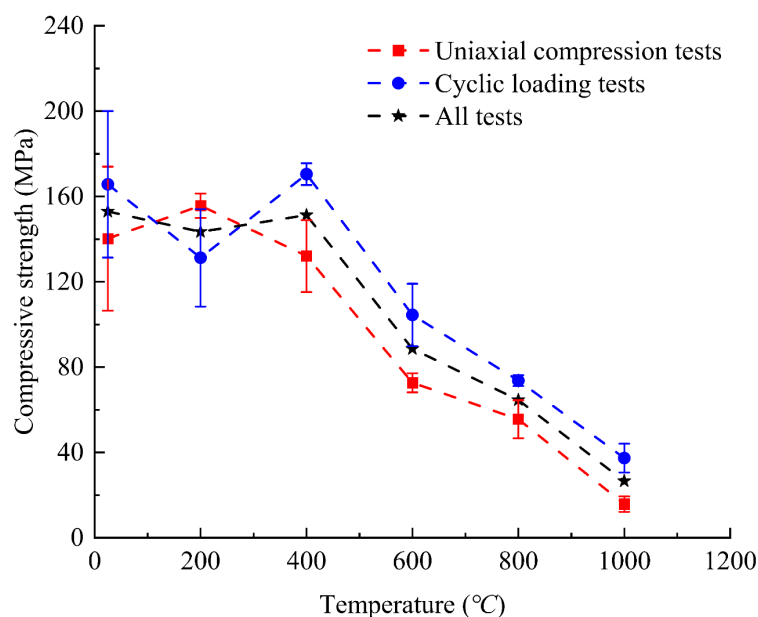

Figure 10. Variations in compressive strength of samples treated at different temperatures.

The compressive strength of specimens in the cyclic loading test is lower than that in the uniaxial compression test at a treatment temperature of 200 °C. However, the compressive strength of specimens treated at other temperatures under cyclic loading is significantly enhanced. Notably, when the treatment temperature reaches 400 °C, the compressive strength of the sample after cyclic loading is increased by 29.1%. This strengthening effect under cyclic loading has also been confirmed by previous studies [51,52]. There are two main reasons for this strengthening effect. First, cyclic loading and unloading in the early stage causes adjustment and compaction of the internal microstructure of the rock. Second, when the axial stress is discharged, the debris formed by the shear slip of the new fracture surface of the rock fills nearby pores, thereby improving the friction between the fracture surfaces and increasing the strength of the rock sample [53,54]. Additionally, compared with samples that are not subjected to thermal treatment, the compressive strength of samples heated at 400 °C under cyclic loading increases. This may be attributed to the combined effects of cyclic loading and the thermal effects [26].

4.3. Crack Damage Threshold

The crack damage threshold σ_{cd} represents the initial stress during the unstable development stage of a crack. It is determined by identifying the inflection point at which the volumetric strain curve of the rock sample transitions from compaction to dilatancy. The method for determining this threshold is illustrated in Figure 11 [55,56].
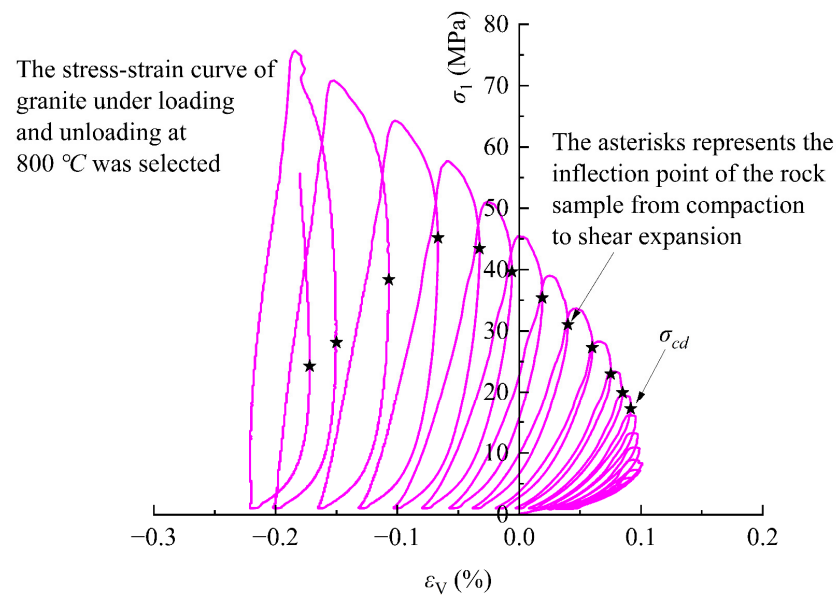
Figure 11. Diagram of the crack damage threshold.

Figure 12 illustrates the variations in the crack damage threshold and the ratio between the crack damage threshold and the average uniaxial compressive strength of specimens (σ_{cd}/σ_c) in the uniaxial compression test at different treatment temperatures. At room temperature (25 °C), σ_{cd} of the sample is 124.64 MPa. However, at a thermal treatment temperature of 200 °C, the crack damage threshold decreases to 95.37 MPa. As the treatment temperature increases to 400 °C, the crack damage threshold increases to 114.26 MPa. Moreover, within the temperature range of 400–1000 °C, the crack damage threshold consistently decreases with increasing treatment temperature, reaching a minimum value of 3.82 MPa at 1000 °C. The trend of σ_{cd}/σ_c with treatment temperature is similar to that of σ_{cd}. However, it is important to note that σ_{cd}/σ_c reaches its maximum value at a treatment temperature of 400 °C, which further supports the notion that the thermal hardening phenomenon strengthens the initial stress of damage at 400 °C.
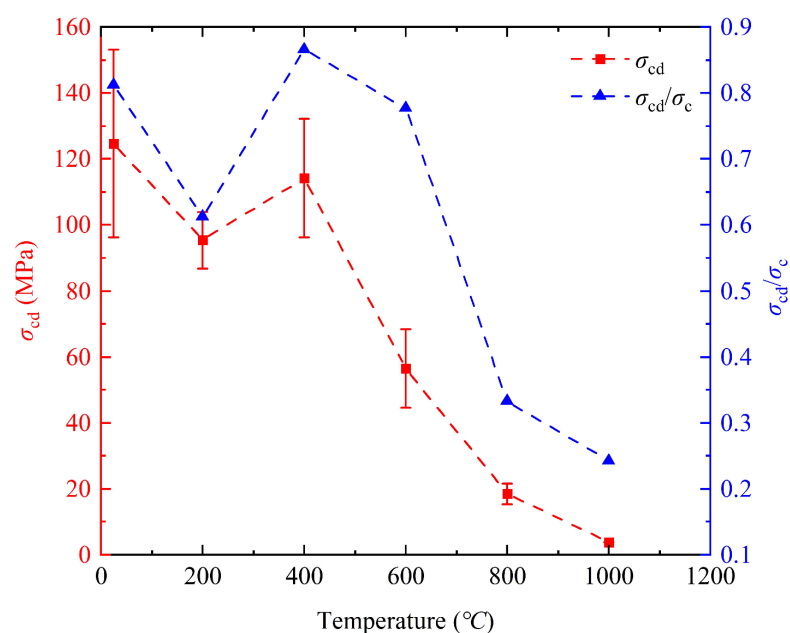

Figure 12. Variations in crack damage thresholds of samples under uniaxial compression tests with treatment temperature.

Figure 13 illustrates the impact of the cycle number on the crack damage threshold evolution in cyclic loading tests. The crack damage threshold of granite samples at different temperatures exhibits similar characteristics. Initially, as the cycle number increases, the crack damage threshold of the sample rises. This can be attributed to the increased difficulty in reopening previously closed cracks after unloading in the previous cycle [57]. Subsequently, σ_{cd} gradually decreases with the cycle number, as new cracks continue to initiate, propagate, and coalesce, leading to the accumulation of damage in the specimen. Furthermore, at temperatures below 25 °C (room temperature) and cycle numbers less than 19, the sample does not transition from compaction to dilatancy, and there is no inflection point in the bulk strain curve. However, the cycle number required for the sample to transform from compaction to dilatancy decreases significantly after thermal treatment. For instance, when the treatment temperature reaches 1000 °C, the cycle number decreases to 9. This suggests that thermal treatment profoundly affects the dilatancy characteristics of granite samples, making dilatancy more likely to occur under cyclic loading.
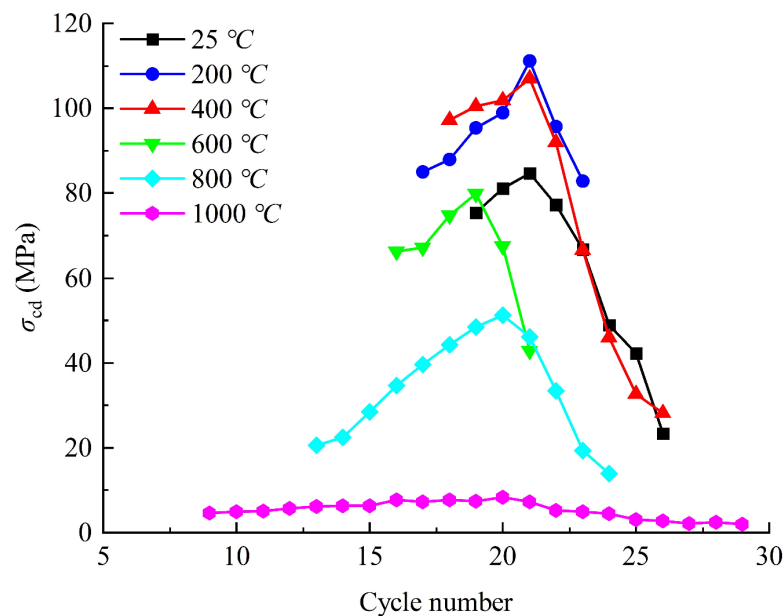

Figure 13. Variations in crack damage thresholds of typical samples heated at different temperatures under uniaxial cyclic loading with cycle number.

4.4. Elastic Properties

Figure 14 illustrates the variations in the elastic modulus *E* of the sample with treatment temperature. The elastic modulus of the sample in the uniaxial compression test is determined by calculating the average slope of the straight section of the stress-strain curve. Similarly, in the cyclic loading test, the elastic modulus is determined by calculating the average slope of the straight section of the outer envelope curve at each unloading point of the stress-strain curve. Generally, the elastic modulus remains relatively constant within the temperature range of 25–400 °C but decreases within the temperature range of 400–1000 °C. This observation aligns with the experimental findings of Zhang et al. [58]. Interestingly, the elastic modulus of the specimen fluctuates when the treatment temperature is between 25 °C and 400 °C under cyclic loading, compared with uniaxial compression. However, when the specimen is treated between 400 °C and 1000 °C, the elastic modulus remains stable and greater than that obtained by the uniaxial compression test. This suggests that the critical temperature for inducing thermal damage in granite is between 400 °C and 600 °C. Thermal damage leads to the initiation of microcracks, while cyclic loading causes the microcracks to close, resulting in the hardening of the sample after treatment at high temperature.
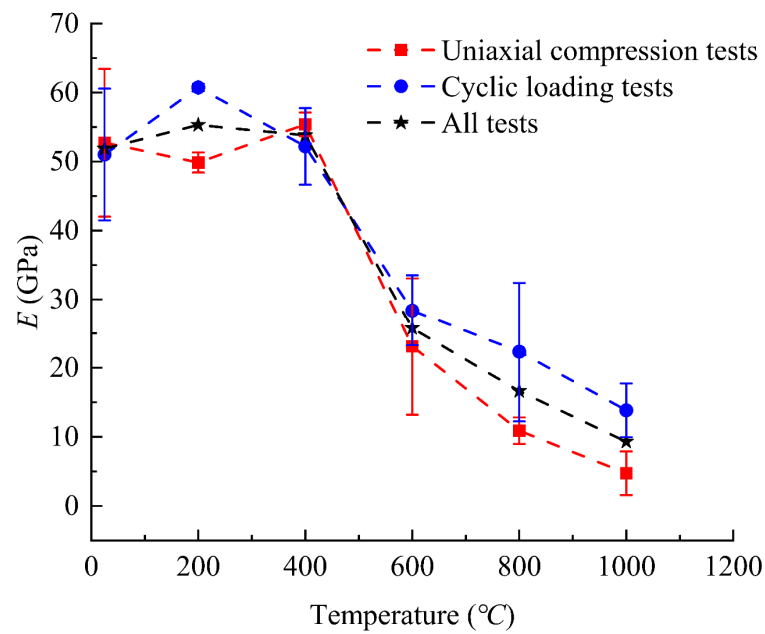
Figure 14. Variations in elastic modulus with treatment temperature.

The methods for determining the loading secant modulus E_i^+ and unloading secant modulus E_i^- of the ith cycle are illustrated in Figure 15, where $\sigma_{i\max}$ and $\sigma_{i\min}$ are the peak stress and initial stress of the ith loading, respectively, and $\varepsilon_{i\max}$, ε_i^+ and ε_i^- are the peak longitudinal strain, initial longitudinal strain, and unloading longitudinal strain of the ith loading, respectively [59,60]. The secant moduli for loading and unloading of typical samples in the cyclic loading test are presented in Figure 16a and Figure 16b, respectively.
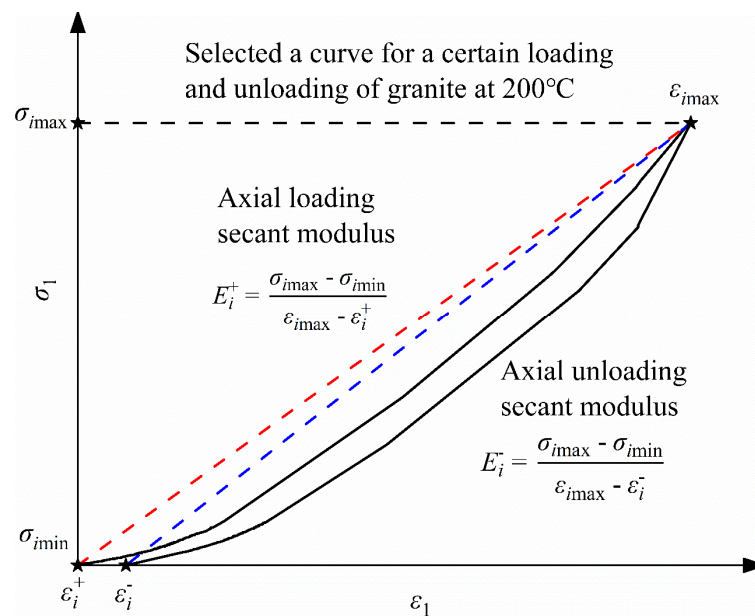

Figure 15. Diagram for determining the loading and unloading secant modulus.
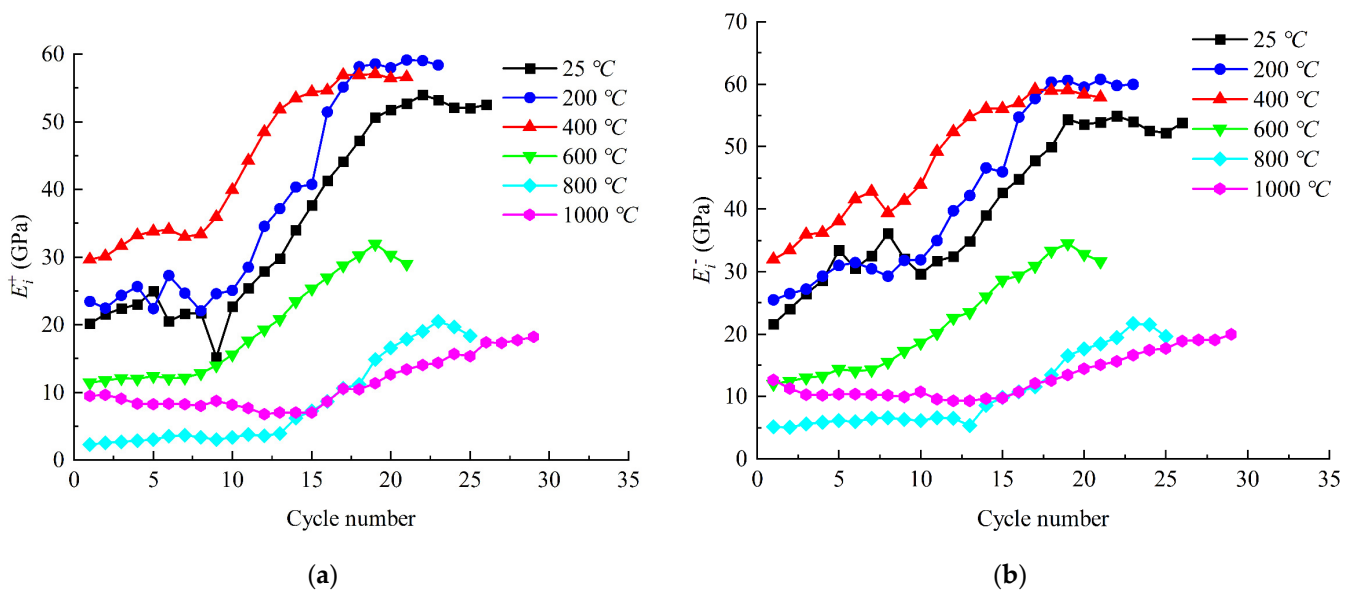
Figure 16. Typical variations in secant modulus of samples heated at different temperatures under uniaxial cyclic loading tests with cycle number: (**a**) loading secant modulus and (**b**) unloading secant modulus.

The evolution of the loading secant modulus E_i^+ can be categorized into three distinct stages. The first stage resembles the initial compaction stage observed in the uniaxial compression test, where the loading modulus remains unchanged or exhibits a gradual increase. The second stage corresponds to the elastic deformation stage observed in the uniaxial compression test, characterized by a nearly linear increase in the loading modulus with each cycle. The third stage corresponds to the yield and post-peak stages observed in the uniaxial compression test, where the loading modulus either remains constant or experiences a slight decrease. The first stage is closely associated with the development level of the initial pores within the sample. During the early stages of cyclic loading, the initial microcracks are closed. In the second stage, the initial crack within the sample becomes compacted and the initiation and compaction of new cracks begin to alternate with cyclic loading. This process gradually increases the stiffness of the sample. In the third stage, the microcracks in the rock connect to form macroscopic cracks. As a result, the increase in the number of cycles does not have a hardening effect on the sample. Once the peak stress is reached, the specimen's bearing capacity is lost and the stiffness of the specimen gradually deteriorates due to cyclic loading until it is ultimately destroyed. When the treatment temperature exceeds 600 °C, the rock sample undergoes thermal damage, resulting in changes in its mineral composition and microstructure. As a consequence, the proportion of the total cycle number in the first stage gradually increases. Additionally, the hardening effect of cyclic loading on the stiffness of the specimen weakens in the second stage. This weakening is reflected in the nonlinear deformation trend observed in the rock sample after thermal treatment.

The trend of variation in the unloading secant modulus E_i^- is similar to that of E_i^+, but the results indicate that E_i^- is slightly larger than E_i^+ in each cycle. This suggests that irreversible plastic deformation occurs during each loading cycle.

4.5. Poisson's Ratio and Lateral Expansion Coefficient

Poisson's ratio u is determined by the ratio of lateral strain to longitudinal strain within the elastic deformation range of the sample. The variation in Poisson's ratio with temperature is illustrated in Figure 17. The Poisson's ratio of the rock sample under cyclic loading and unloading is determined by the ratio of lateral strain to longitudinal strain in the elastic section of the outer envelope curve at each unloading point. For

the sample subjected to cyclic loading, there is a significant dispersion in results. This observation was also made by Zhang et al. [58]. The dispersion may be attributed to the discontinuous and complex displacement of microcracks under cyclic loading [28]. Additionally, the anisotropy of rock samples and the alteration in mineral composition after thermal treatment at different temperatures could also contribute to the notable dispersion [61]. However, with the exception of the samples treated at 200 °C, the Poisson ratios of the samples significantly increase after cyclic loading compared with monotonic loading. This suggests that cyclic loading fully expands the lateral deformation of the sample. Additionally, the Poisson ratio of the sample increases significantly when the treatment temperature exceeds 600 °C. There are two main reasons for this phenomenon. First, the change in the mineral composition of the rock sample after treatment at high temperature reduces the cohesion between mineral particles, making the rock sample more susceptible to lateral deformation under external loading. Second, the initiation of thermally induced microcracks causes the deformation of the sample to spread along the macrocracks, including lateral cracks.
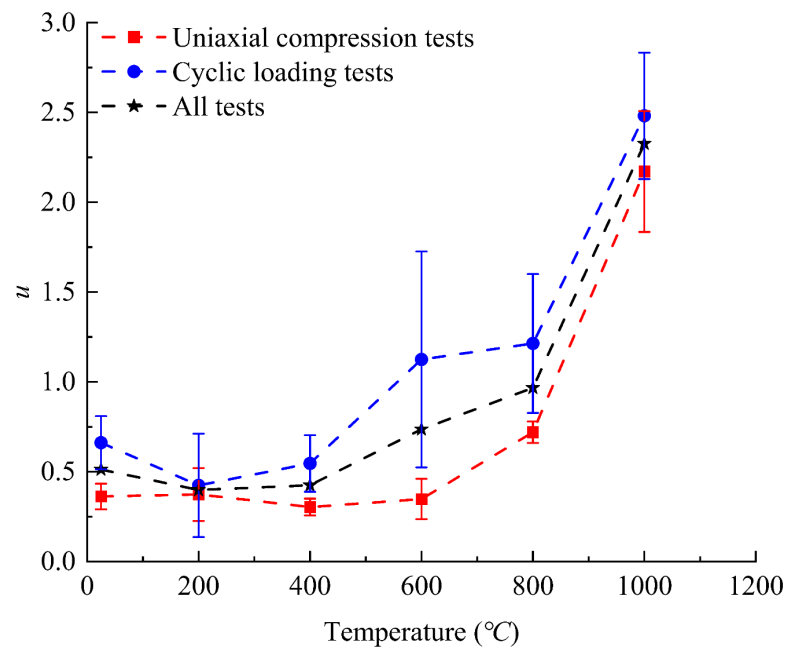

Figure 17. Variations in Poisson's ratio with treatment temperature.

To characterize the overall deformation of rocks and comprehensively analyze the deformation characteristics of granite under cyclic loading, the lateral expansion coefficient is introduced. The method for determining the lateral expansion coefficient u_i of the ith cycle is illustrated in Figure 18, where $\varepsilon_{1i\max}$, $\varepsilon_{1i\min}$, $\varepsilon_{3i\max}$, and $\varepsilon_{3i\min}$ are the peak longitudinal strain, initial longitudinal strain, peak lateral strain, and initial lateral strain of the ith loading, respectively. The lateral expansion coefficient u_i of typical samples in the cyclic loading test changes with the cycle number, as shown in Figure 19. As depicted in the figure, the lateral expansion coefficient consistently increases with the cycle number. Additionally, the slope of the curve representing the lateral expansion coefficient versus the cycle number gradually intensifies as the cycle number approaches damage to the specimen. This phenomenon can be attributed to the fact that an increase in the cycle number weakens the crack tip of the rock sample, making it more susceptible to crack initiation and propagation. Consequently, the lateral expansion coefficient experiences a more rapid increase [60]. The variations in the trends of the lateral expansion coefficient for samples treated at different temperatures are highly similar across different cycle numbers. Only the samples treated at 1000 °C exhibit a substantial disparity, as both the initial value and the range of increase for the lateral expansion coefficient rise significantly. This

discrepancy can be attributed to the transformation of the rock-forming mineral quartz from β to scale quartz at 870 °C, leading to additional alterations in the composition and microstructure of the rock samples [34,62].
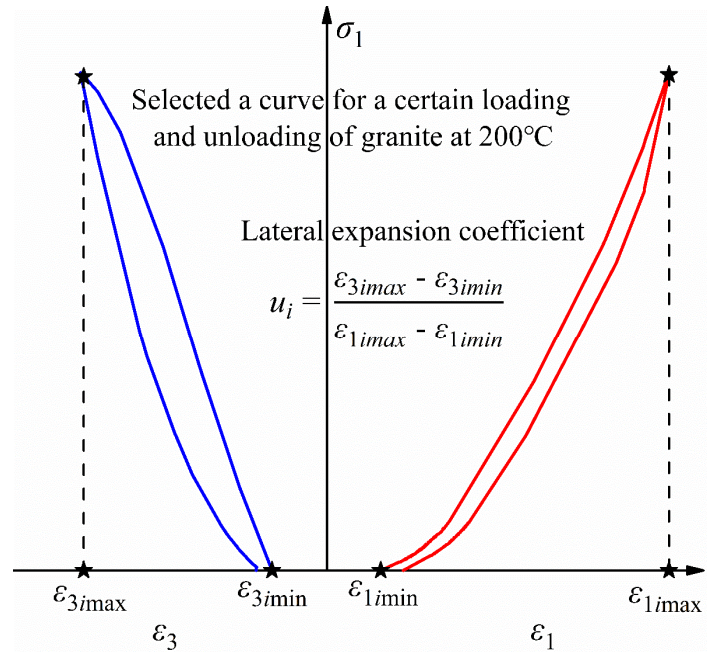

Figure 18. Diagram of lateral expansion coefficient and unloading lateral expansion coefficient.
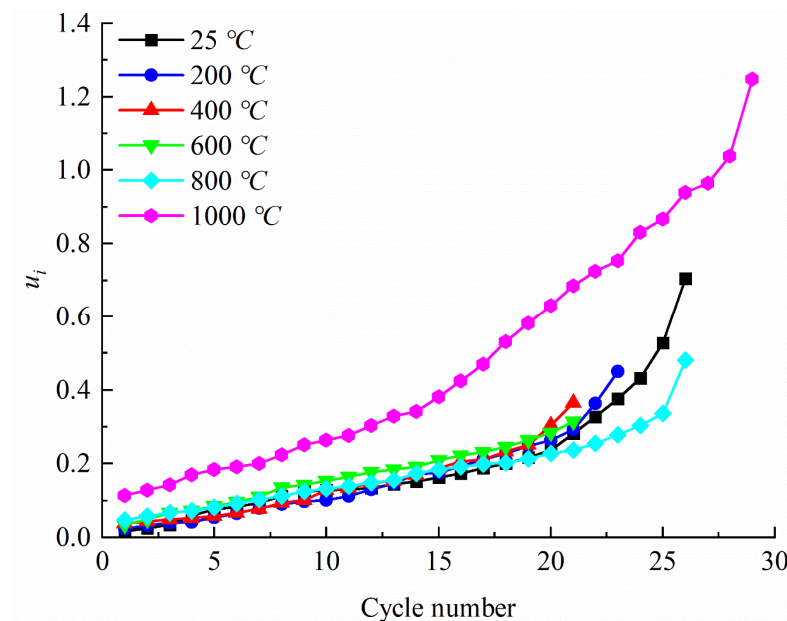
$$u_i = \frac{\varepsilon_{3imax} - \varepsilon_{3imin}}{\varepsilon_{1imax} - \varepsilon_{1imin}}$$

Figure 19. Typical variations in lateral expansion coefficient of samples treated at different temperatures with cycle number.

5. Failure Modes

Figure 20 illustrates the failure patterns observed in typical rock samples. The findings indicate that, under normal temperature conditions, the primary mode of fracture in the rock is tensile splitting. However, when the temperature drops below 400 °C, the predominant fracture form shifts to X-shaped shear fractures. In the temperature range of 600–800 °C, Y-shaped shear fractures become dominant. Furthermore, at a treatment

temperature of 1000 °C, conical fractures prevail in the specimen, accompanied by cataclastic flow. This suggests a transition in the failure mode of the rock specimen from brittle to ductile failure as the treatment temperature increases. The reason for this transformation could be attributed to the propagation of microcracks induced by elevated temperatures and variations in the composition of the rock, consequently modifying the failure mechanisms of the rock [63,64]. At the same time, when compared to uniaxial compression, the degree of damage in the specimen under cyclic loading is higher and the failure pattern is more complex. This is due to the repeated friction caused by cyclic loading, which disrupts the original internal microstructure of the specimen, resulting in the formation of more cracks and failure surfaces within it.
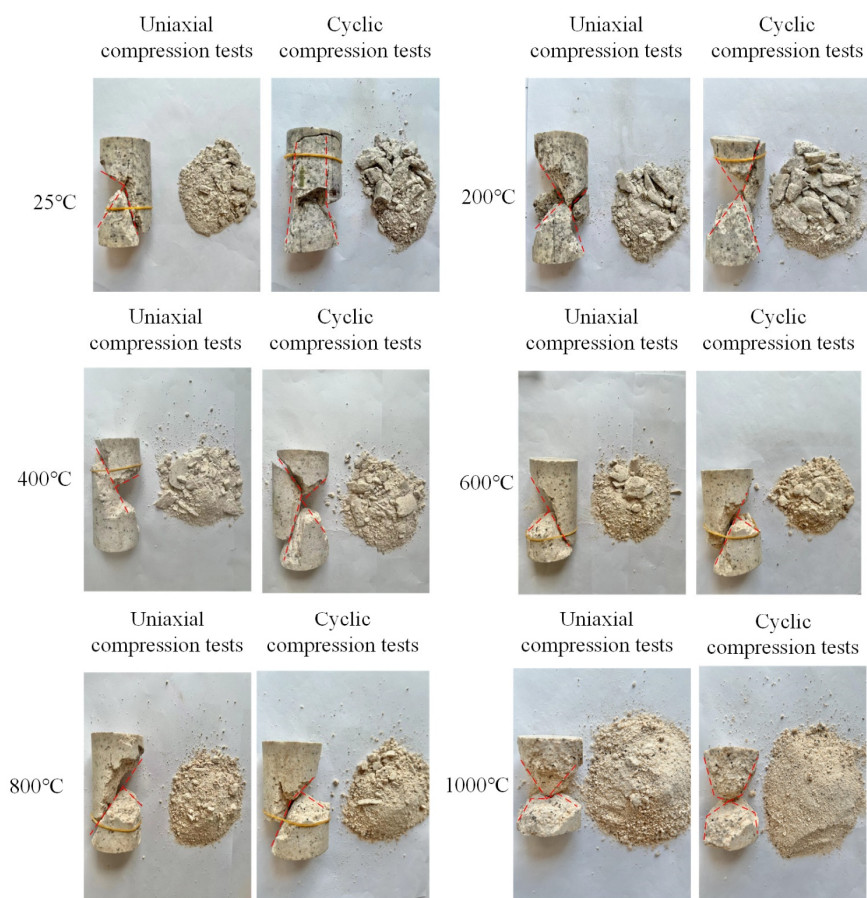

Figure 20. Failure patterns in typical samples. Red lines represent the main cracks formed in the damaged specimens.

In addition, as the treatment temperature increases, small cracks develop on the failure surfaces. These cracks gradually become rough, resulting in loose and easily spalled rock fragments. The rock fragments formed after damage become progressively looser and finer with increasing treatment temperature. At 1000 °C, all the rock fragments are in powder form.

6. Conclusions

In this study, we conducted the uniaxial compression test and the constant lower limit cyclic loading and unloading test on granite samples that were treated at six different temperatures: room temperature, 200 °C, 400 °C, 600 °C, 800 °C, and 1000 °C. Based on the results, the following conclusions can be drawn:

1. The rate of mass loss as the thermal treatment temperature increases can be categorized into three stages. In the initial stage, the rate of mass loss exhibits the greatest variation

within the temperature range of 25–200 °C. In the second stage, the rate of mass loss growth decreases as the treatment temperature ranges from 200 °C to 400 °C. In the third stage, within the treatment temperature range of 400–1000 °C, the rate of mass loss growth rebounds and stabilizes. The change in the rate of volume expansion is not significant when the treatment temperature is below 400 °C, but it increases rapidly once the treatment temperature exceeds 400 °C.

2. The nonlinearity of the stress-strain curve is intensified by elevating the treatment temperature, resulting in a prolonged nonlinear compaction stage during uniaxial compression. When subjected to cyclic loading conditions, an increase in treatment temperature leads to a sparser hysteresis loop and greater plastic deformation. Furthermore, the treatment temperature significantly impacts the compressive strength of the specimen. Specifically, the compressive strength increases within the temperature range of 200–400 °C but experiences a sharp decline beyond 400 °C.

3. Thermal treatment significantly affects the dilatation characteristics of granite. The crack damage threshold reaches its peak at 400 °C and decreases consistently as the treatment temperature increases from 400 °C to 1000 °C. When subjected to cyclic loading, thermal treatment greatly reduces the number of cycles needed for the sample to transition from compaction to dilatancy.

4. The elastic modulus remains relatively constant within the temperature range of 25–400 °C but decreases within the range of 400–1000 °C. Additionally, the relationship between the elastic moduli of specimens subjected to uniaxial compression and cyclic loading is unclear within the temperature range of 25–400 °C. However, the elastic moduli of specimens treated within the temperature range of 400–1000 °C are generally greater under cyclic loading compared with uniaxial compression.

5. The Poisson's ratio of the specimen starts to increase with the treatment temperature, surpassing 200 °C. The increase is more pronounced under cyclic loading. The trend of the lateral expansion coefficient with the number of cycles is similar for samples treated at different temperatures. However, the samples heated at 1000 °C exhibit a notable difference, with a significant increase in both the initial value and the range of the lateral expansion coefficient.

Based on the analyses above, it can be concluded that rocks that have undergone thermal treatment are more susceptible to deformation and failure. This poses significant safety risks when conducting deep geothermal energy development or high-temperature rock underground engineering. When the temperature exceeds 400 °C, the strength of the rock significantly decreases. Therefore, it is not recommended to subject the rock to thermal treatment at temperatures above 400 °C. However, it is important to note that the complexity of rock structures and the limitations of the testing method may have led to data discreteness during the testing process. Additionally, the influence of variations between individual samples on the test results cannot be disregarded. Therefore, further tests are necessary to validate the findings presented in this article. Specifically, exploring the long-term effects of cyclic loading after thermal treatment could serve as a basis for future investigations.

Institutional Review Board Statement: Not applicable.

Informed Consent Statement: Not applicable.

Conflicts of Interest: The authors declare no conflict of interest.

References

1. Vagnon, F.; Colombero, C.; Colombo, F.; Comina, C.; Ferrero, A.M.; Mandrone, G.; Vinciguerra, S.C. Effects of thermal treatment on physical and mechanical properties of Valdieri Marble—NW Italy. *Int. J. Rock Mech. Min. Sci.* **2019**, *116*, 75–86. [CrossRef]
2. Chen, W.; Wan, W.; Zhao, Y.; Peng, W. Experimental study of the crack predominance of rock-like material containing parallel double fissures under uniaxial compression. *Sustainability* **2020**, *12*, 5188. [CrossRef]
3. Wu, H.; Jia, Q.; Wang, W.J.; Zhang, N.; Zhao, Y.M. Experimental test on nonuniform deformation in the tilted strata of a deep coal mine. *Sustainability* **2021**, *13*, 13280. [CrossRef]
4. Zhang, Y.L.; Zhao, G.F. A global review of deep geothermal energy exploration: From a view of rock mechanics and engineering. *Geomech. Geophys. Geo-Energy Geo-Resour.* **2020**, *6*, 26. [CrossRef]
5. McClure, M.W.; Horne, R.N. Correlations between formation properties and induced seismicity during high pressure injection into granitic rock. *Eng. Geol.* **2014**, *175*, 74–80. [CrossRef]
6. Moska, R.; Labus, K.; Kasza, P. Hydraulic Fracturing in Enhanced Geothermal Systems-Field, Tectonic and Rock Mechanics Conditions-A Review. *Energies* **2021**, *14*, 24. [CrossRef]
7. Wu, X.H.; Guo, Q.F.; Li, P.; Ren, F.H.; Zhang, J.; Cai, M.F. Investigating the Effect of Temperature Changes on the Physical Field of Surrounding Rock in a Deep Gold Mine. *Adv. Mater. Sci. Eng.* **2021**, *2021*, 13. [CrossRef]
8. Zhao, Y.L.; Liu, J.H.; Zhang, H.Q.; Liao, J.; Zhu, S.T.; Zhang, L.Y. Mechanical behavior of sandstone during post-peak cyclic loading and unloading under hydromechanical coupling. *Int. J. Min. Sci. Technol.* **2023**, *33*, 927–947. [CrossRef]
9. Li, C.; Hu, Y.Q.; Zhang, C.W.; Zhao, Z.R.; Jin, P.H.; Hu, Y.F.; Zhao, G.K. Brazilian split characteristics and mechanical property evolution of granite after cyclic cooling at different temperatures. *Chin. J. Rock Mech. Eng.* **2020**, *39*, 1797–1807.
10. Yuan, Z.; Zhao, J.; Li, S.; Jiang, Z.; Huang, F. A unified solution for surrounding rock of roadway considering seepage, dilatancy, strain-softening and intermediate principal stress. *Sustainability* **2022**, *14*, 8099. [CrossRef]
11. Zhao, Y.L.; Tang, J.Z.; Chen, Y.; Zhang, L.Y.; Wang, W.J.; Wan, W.; Liao, J.P. Hydromechanical coupling tests for mechanical and permeability characteristics of fractured limestone in complete stress–strain process. *Environ. Earth Sci.* **2017**, *76*, 1866–6280. [CrossRef]
12. Zhao, Y.L.; Liu, Q.; Zhang, C.S.; Liao, J.; Lin, H.; Wang, Y.X. Coupled seepage-damage effect in fractured rock masses: Model development and a case study. *Int. J. Rock Mech. Min. Sci.* **2021**, *144*, 1365–1609. [CrossRef]
13. Zhao, Y.L.; Wang, Y.X.; Wang, W.J.; Tang, L.M.; Liu, Q.; Cheng, G.M. Modeling of rheological fracture behavior of rock cracks subjected to hydraulic pressure and far field stresses. *Theor. Appl. Fract. Mech.* **2019**, *101*, 0167–8442. [CrossRef]
14. Zhou, X.Y.; Sun, D.A.; Luo, T. Semi-analytical solution of near-field temperature in nuclear waste disposal repository. *Rock Soil Mech.* **2020**, *41* (Suppl. S1), 246–254.
15. Li, P.; Cai, M.F. Challenges and new insights for exploitation of deep underground metal mineral resources. *Trans. Nonferrous Met. Soc. China* **2021**, *31*, 3478–3505. [CrossRef]
16. Zhuang, L.; Kim, K.Y.; Jung, S.G.; Diaz, M.; Min, K.B.; Zang, A.; Stephansson, O.; Zimmerman, G.; Yoon, J.S.; Hofmann, H. Cyclic hydraulic fracturing of pocheon granite cores and its impact on breakdown pressure, acoustic emission amplitudes and injectivity. *Int. J. Rock Mech. Min. Sci.* **2019**, *122*, 9. [CrossRef]
17. Zhao, G.K.; Hu, Y.Q.; Jin, P.H.; Hu, Y.F.; Li, C.; Zhu, X.Z. Experimental study on mechanical properties of granite subjected to cyclic loads under real time temperature. *Chin. J. Rock Mech. Eng.* **2019**, *38*, 927–937.
18. Kumari, W.G.P.; Ranjith, P.G.; Perera, M.S.A.; Shao, S.; Chen, B.K.; Lashin, A.; Al Arifi, N.; Rathnaweera, T.D. Mechanical behaviour of Australian Strathbogie granite under in-situ stress and temperature conditions: An application to geothermal energy extraction. *Geothermics* **2017**, *65*, 44–59. [CrossRef]
19. Xu, X.L.; Gao, F.; Zhang, Z.Z.; Chen, L. Experimental study of the effect of loading rates on mechanical properties of granite at real-time high temperature. *Rock Soil Mech.* **2015**, *36*, 2184–2192.
20. Gautam, P.K.; Verma, A.K.; Jha, M.K.; Sharma, P.; Singh, T.N. Effect of high temperature on physical and mechanical properties of Jalore granite. *J. Appl. Geophys.* **2018**, *159*, 460–474. [CrossRef]
21. Wu, Q.H.; Weng, L.; Zhao, Y.L.; Guo, B.H.; Luo, T. On the tensile mechanical characteristics of fine-grained granite after heating/cooling treatments with different cooling rates. *Eng. Geol.* **2019**, *253*, 94–110. [CrossRef]
22. Yin, T.B.; Shu, R.H.; Li, X.B.; Wang, P.; Liu, X.L. Comparison of mechanical properties in high temperature and thermal treatment granite. *Trans. Nonferrous Met. Soc. China* **2016**, *26*, 1926–1937. [CrossRef]
23. Zhou, H.W.; Wang, Z.H.; Wang, C.S.; Liu, J.F. On Acoustic Emission and Post-peak Energy Evolution in Beishan Granite Under Cyclic Loading. Rock Mech. *Rock Eng.* **2019**, *52*, 283–288. [CrossRef]
24. Chen, Y.L.; Ni, J.; Shao, W.; Azzam, R. Experimental study on the influence of temperature on the mechanical properties of granite under uni-axial compression and fatigue loading. *Int. J. Rock Mech. Min. Sci.* **2012**, *56*, 62–66. [CrossRef]

25. Jia, P.; Wang, Y.; Li, B.; Qian, Y.J. Experimental Study on Mechanical Properties of Water-Cooled High Temperature Rock Under Cyclic Loading. *Trans. Beijing Inst. Technol.* **2023**, *43*, 126–134.

26. Xia, C.C.; Zhou, S.W.; Hu, Y.S.; Zhang, P.Y.; Zhou, Y. Preliminary study on mechanical property of basalt subjected to cyclic uniaxial stress and cyclic temperature. *Chin. J. Geotech. Eng.* **2015**, *37*, 1016–1024.

27. Zhao, G.K.; Guo, Y.T.; Chang, X.; Jin, P.H.; Hu, Y.Q. Effects of temperature and increasing amplitude cyclic loading on the mechanical properties and energy characteristics of granite. *Bull. Eng. Geol. Environ.* **2022**, *81*, 13. [CrossRef]

28. Han, D.Y.; Li, K.H. Physico-mechanical properties and brittle to plastic transition of a thermally cracked marble under uniaxial tension. *Geothermics* **2023**, *109*, 13. [CrossRef]

29. Ulusay, R. *The ISRM Suggested Methods for Rock Characterization, Testing and Monitoring: 2007–2014*; Springer International Publishing: Cham, Switzerland, 2015; pp. 51–68.

30. Zhang, W.Q.; Sun, Q.; Hao, S.Q.; Geng, J.S.; Lv, C. Experimental study on the variation of physical and mechanical properties of rock after high temperature treatment. *Appl. Therm. Eng.* **2016**, *98*, 1297–1304. [CrossRef]

31. Yin, T.B.; Li, X.B.; Yin, Z.Q.; Zhou, Z.L.; Liu, X.L. Study and comparison of mechanical properties of sandstone under static and dynamic loadings after high temperature. *Chin. J. Rock Mech. Eng.* **2012**, *31*, 273–279.

32. Zuo, J.P.; Xie, H.P.; Zhou, H.W.; Peng, S.P. SEM in situ investigation on thermal cracking behaviour of Pingdingshan sandstone at elevated temperatures. *Geophys. J. Int.* **2010**, *181*, 593–603.

33. Wu, X.H.; Cai, M.F.; Ren, F.H.; Sun, J.L.; Guo, Q.F.; Wu, X.; Zhang, J.; Zhang, L.W. P-wave evolution and thermal conductivity characteristics in granite under different thermal treatment. *Chin. J. Rock Mech. Eng.* **2022**, *41*, 457–467.

34. Sun, Q.; Zhang, Z.Z.; Xue, L.; Zhu, S.Y. Physical-mechanical properties variation of rock with phase transformation under high temperature. *Chin. J. Rock Mech. Eng.* **2013**, *32*, 935–942.

35. Sun, H.; Sun, Q.; Deng, W.N.; Zhang, W.Q.; Lu, C. Temperature effect on microstructure and P-wave propagation in Linyi sandstone. *Appl. Therm. Eng.* **2017**, *115*, 913–922. [CrossRef]

36. Ohno, I. Temperature variation of elastic properties of α-quartz up to the α-β transition. *J. Phys. Earth* **1995**, *43*, 157–169. [CrossRef]

37. Zhao, X.G.; Zhao, Z.; Guo, Z.; Cai, M.; Li, X.; Li, P.F.; Chen, L.; Wang, J. Influence of Thermal Treatment on the Thermal Conductivity of Beishan Granite. Rock Mech. *Rock Eng.* **2018**, *51*, 2055–2074. [CrossRef]

38. Ferrero, A.M.; Marini, P. Experimental studies on the mechanical behaviour of two thermal cracked marbles. *Rock Mech. Rock Eng.* **2001**, *34*, 57–66. [CrossRef]

39. Liu, S.; Xu, J.Y. An experimental study on the physico-mechanical properties of two post-high-temperature rocks. *Eng. Geol.* **2015**, *185*, 63–70. [CrossRef]

40. Li, C.X. Optimum multiple tuned mass dampers for structures under the ground acceleration based on DDMF and ADMF. *Earthq. Eng. Struct. Dyn.* **2002**, *31*, 897–919. [CrossRef]

41. Zhi, L.P.; Xu, J.Y.; Liu, J.Z.; Liu, S.; Chen, T.F. Research on ultrasonic characteristics and mechanical properties of granite under post-hightemperature. *Chin. J. Undergr. Space Eng.* **2012**, *8*, 716–721.

42. Zong, Y.; Han, L.; Wei, J.; Wen, S. Mechanical and damage evolution properties of sandstone under triaxial compression. *Int. J. Min. Sci. Technol.* **2016**, *26*, 601–607. [CrossRef]

43. Meng, Q.S.; Wang, C.K.; Huang, B.X.; Pu, H.; Zhang, Z.Z.; Sun, W.; Wang, J. Rock energy evolution and distribution law under triaxial cyclic loading and unloading conditions. *Chin. J. Rock Mech. Eng.* **2020**, *39*, 13.

44. Heap, M.J.; Faulkner, D.R. Quantifying the evolution of static elastic properties as crystalline rock approaches failure. *Int. J. Rock Mech. Min. Sci.* **2008**, *45*, 564–573. [CrossRef]

45. Xiao, F.K.; Shen, Z.L.; Liu, G.; Zhang, Z.Z.; Zhang, F.R. Relationship between hysteresis loop and elastoplastic strain energy during cyclic loading and unloading. *Chin. J. Rock Mech. Eng.* **2014**, *33*, 1791–1797.

46. Rao, G.M.N.; Murthy, C.R.L. Dual role of microcracks: Toughening and degradation. *Can. Geotech. J.* **2001**, *38*, 427–440. [CrossRef]

47. Sirdesai, N.N.; Singh, T.N.; Ranjith, P.G.; Singh, R. Effect of Varied Durations of Thermal Treatment on the Tensile Strength of Red Sandstone. Rock Mech. *Rock Eng.* **2017**, *50*, 205–213. [CrossRef]

48. Li, M.; Mao, X.B.; Cao, L.L.; Pu, H.; Mao, R.R.; Lu, A.H. Effects of Thermal Treatment on the Dynamic Mechanical Properties of Coal Measures Sandstone. Rock Mech. *Rock Eng.* **2016**, *49*, 3525–3539. [CrossRef]

49. Yang, S.Q.; Ranjith, P.G.; Jing, H.W.; Tian, W.L.; Ju, Y. An experimental investigation on thermal damage and failure mechanical behavior of granite after exposure to different high temperature treatments. *Geothermics* **2017**, *65*, 180–197. [CrossRef]

50. Yin, T.B.; Li, X.B.; Cao, W.Z.; Xia, K.W. Effects of Thermal Treatment on Tensile Strength of Laurentian Granite Using Brazilian Test. Rock Mech. *Rock Eng.* **2015**, *48*, 2213–2223. [CrossRef]

51. Zhang, X.; Yu, H.; Li, Z.; Liu, Y.S.; Zhang, Z.D.; Ji, X.Y.; Li, X.H. Discrete element study on effect of cyclic loading strengthening on meso-destruction of granite. *J. Zhejiang Univ. (Eng. Sci.)* **2022**, *56*, 2303–2312.

52. Xu, S.C.; Feng, X.T.; Chen, B.R. Experimental study of skarn under uniaxial cyclic loading and unloading test and acoustic emission characteristics. *Rock Soil Mech.* **2009**, *30*, 2929–2934.

53. You, Q.M.; Su, C.D. Experimental research on strengthening under cyclic loading of marble samples. *Chin. J. Solid Mech.* **2008**, *29*, 66–72.

54. Zhou, J.W.; Yang, X.G.; Fu, W.X.; Xu, J.; Li, H.T.; Zhou, H.W.; Liu, J.F. Experimental test and fracture damage mechanical characteristics of brittle rock under uniaxial cyclic loading and unloading conditions. *Chin. J. Rock Mech. Eng.* **2010**, *29*, 1172–1183.

55. Wong, T.f.; David, C.; Zhu, W. The transition from brittle faulting to cataclastic flow in porous sandstones: Mechanical deformation. *J. Geophys. Res. Solid Earth* **1997**, *102*, 3009–3025. [CrossRef]

56. Yang, S.Q.; Liu, X.R. Experimental investigation on dilatancy behavior of marble with pre-existing fissures under different confining pressures. *Chin. J. Geotech. Eng.* **2012**, *34*, 2188–2197.

57. Yang, S.Q.; Ranjith, P.G.; Huang, Y.H.; Yin, P.F.; Jing, H.W.; Gui, Y.L.; Yu, Q.L. Experimental investigation on mechanical damage characteristics of sandstone under triaxial cyclic loading. *Geophys. J. Int.* **2015**, *201*, 662–682. [CrossRef]

58. Zhang, F.; Zhao, J.J.; Hu, D.W.; Skoczylas, F.; Shao, J.F. Laboratory Investigation on Physical and Mechanical Properties of Granite After Heating and Water-Cooling Treatment. Rock Mech. *Rock Eng.* **2018**, *51*, 677–694. [CrossRef]

59. Chen, S.W.; Liang, F.; Zuo, S.Y.; Wu, D.Y. Evolution of deformation property and strength component mobilization for thermally treated Beishan granite under compression. *J. Cent. South Univ.* **2021**, *28*, 219–234. [CrossRef]

60. Li, X.W.; Yao, Z.S.; Huang, X.W.; Liu, Z.X.; Zhao, X.; Mu, K.H. Investigation of deformation and failure characteristics and energy evolution of sandstone under cyclic loading and unloading. *Rock Soil Mech.* **2021**, *42*, 12.

61. Gautam, P.K.; Jha, M.K.; Verma, A.K.; Singh, T.N. Experimental study of thermal damage under compression and tension of Makrana marble. *J. Therm. Anal. Calorim.* **2020**, *139*, 609–627. [CrossRef]

62. Zhang, Z.Z.; Gao, F.; Xu, X.L. Acoustic emission characteristics and themodynamic coupling model of granite under uniaxial compression. *Chin. J. Undergr. Space Eng.* **2010**, *6*, 5.

63. Wen, T.; Wang, Y.; Tang, H.; Zhang, J.; Hu, M. Damage Evolution and Failure Mechanism of Red-Bed Rock under Drying–Wetting Cycles. *Water* **2023**, *15*, 2684. [CrossRef]

64. Tao, W.; Tang, H.; Wang, Y.; Ma, J. Evaluation of methods for determining rock brittleness under compression. *J. Nat. Gas Sci. Eng.* **2020**, *78*, 1875–5100. [CrossRef]